IEEE Access
Multidisciplinary | Rapid Review | Open Access Journal

Received October 22, 2017, accepted November 22, 2017, date of publication January 2, 2018,
date of current version February 28, 2018.

Digital Object Identifier 10.1109/ACCESS.2017.2787689

Detection of Salt and Sugar Contents in Water on the Basis of Dielectric Properties Using Microstrip Antenna-Based Sensor

MOHAMMAD TARIQUL ISLAM[1,2], (Senior Member, IEEE),
MD. NAIMUR RAHMAN[1], (Student Member, IEEE),
MANDEEP SINGH JIT SINGH[1], (Member, IEEE),
AND MD. SAMSUZZAMAN[1], (Student Member, IEEE)

[1]Department of Electrical, Electronic and Systems Engineering, Universiti Kebangsaan Malaysia, Bangi 43600, Malaysia
[2]Kyushu Institute of Technology, Kitakyushu 804-8550, Japan

Corresponding author: Mohammad Tariqul Islam (tariqul@ukm.edu.my) and Md. Naimur Rahman (p86256@siswa.ukm.edu.my)

This work was supported by the University Research Grant of the Universiti Kebangsaan Malaysia under the Grant DIP-2017-014.

ABSTRACT This paper presents a microstrip antenna-based sensor for detecting salt and sugar in water. The patch antenna is low-cost and low-profile and is modeled to transmit and receive an electromagnetic signal. The presented antenna consists of a crescent-shaped patch and slotted partial ground. The compact size of the antenna is 32 mm × 22 mm. High-frequency structure simulator and computer simulation technology are used to simulate and analyze the characteristics of the antenna. The presented antenna achieves a 10 dB return loss from 2.50 to 18 GHz with 6.10 dBi of maximum gain, considerable efficiency, and consistent radiation patterns. The presented antenna is used as a sensor to detect salt and sugar in water in terms of reflection coefficient based on the dielectric properties of the solution. The percentage of salt and sugar in water changes the dielectric properties of the solution and the reflection coefficients subsequently. Results during the practical observations show that the reflection coefficient decreases with the increment of salt and sugar contents in the solution. With the excellent basic wideband antenna performances, the antenna shows good sensitivity to detect salt and sugar content in water. The presented antenna is suitable to be used in wideband wireless communications as well as wideband sensor applications.

INDEX TERMS Dielectric properties, microstrip patch antenna, salinity, sensor, sugar.

I. INTRODUCTION

In the recent era, human beings have been facing diseases, such as diabetes, stroke, and kidney failures, because of food and beverages containing superfluous salt and sugar. Few procedures have been established to determine salt and sugar contents in food and beverages. A conventional drying method has been reported in [1] to measure salt in soil by measuring the electrical conductivity of the soil solution. An open-ended coaxial probe has been used through microwave measurement technique to sense the dielectric concentration of starch in a salt– starch solution [2]. However, these procedures remain comparatively complex and time-consuming, and the system development cost of these procedures is high. Currently, microstrip technology is extensively used in various fields, such as agriculture, medicine, sensor, and communications, to overcome the abovementioned abridgments. [2]–[12]. Dielectric-based sensors have been broadly studied and used to detect moisture content, temperature, bulk density, salinity, fuel adulteration, and sugar content in water. These sensors depend on the dielectric and physical characteristics of the material. A technique for quantifying the effects of salinity on the dielectric properties of water has been described in [3]. However, this technique has been used only in 200 MHz–1.4 GHz frequency band. The microstrip-based patch antenna has been utilized in measuring the dielectric properties of materials that are operated only at the low frequency of 433 MHz. Moreover, the environment has been significantly affecting the antenna performance in practical usage when fiberglass is used as a substrate [4]. The waveguide probes and reflection method-based technique of medical diagnostics have been used to determine the dielectric properties of biological tissues [5]. The rectangular dielectric waveguide technique has been described in [6] for calculating moisture content in oil of palm

fruits in the 8 GHz–12 GHz frequency band. A U-shaped microstrip patch antenna, which is referenced in [7], has been presented for detecting moisture content in Hevea rubber latex. A dual frequency microwave moisture sensor has been described on the basis of the circular microstrip antenna [8]. In [9], a microstrip-based patch antenna, which is operated in 0.5–5 GHz, has been referenced to calculate the moisture content in Hevea rubber latex. A single-chip wireless humidity sensor capable of sensing humidity at 37 °C has been rendered in [10]. A metamaterial-inspired microfluidic sensor based on the split-ring resonator, in which the resonance frequency depends on the dielectric properties of the fluid, has been reported [11]. An aligned- and centered-gap rectangular multiple split-ring resonators for the dielectric sensor applications have been implemented [12]. This metamaterial sensor has been used only at 5 GHz with a size of 35 mm × 14 mm. Several procedures mentioned in the literature review are used to detect the moisture and soluble solid contents in agricultural products. However, these methods are time-consuming and cause errors during the measurement.

In this paper, a compact crescent-shaped antenna with a dimension of 32 mm × 22 mm × 1.60 mm is presented. The presented antenna covers the frequency band from 2.50 GHz to 18 GHz, thereby maintaining a VSWR ≤ 2. The antenna has a maximum gain of 6.1 dBi, considerable efficiency, and stable radiation pattern throughout the operating bandwidth. The presented antenna is used to detect salt and sugar contents in water. This microstrip-based antenna sensor is easy to design and fabricate. The development of the measurement system is simple and easy to establish.

II. OPERATING PRINCIPLE OF MICROSTRIP PATCH ANTENNA AS SENSOR

The fringing field from the patch to the substrate causes the electromagnetic radiation from the microstrip patch to the substrate. Thus, the permittivity of the substrate and the patch size directly affects the performances of the patch sensor. A coaxial or probe feeding technique is used to provide signal sources to the patch. In this feeding mechanism, the feed is directly attached to the patch to reduce the fraudulent radiation; hence the antenna can operate at a large bandwidth. The performances of the microstrip patch antenna depend on several factors, such as patch size and shape. The patch size changes the resonance frequency of the microstrip antenna. In this work, the working principle of the sensor is to measure the reflection coefficient of the sensing antenna within the different concentrated salt and sugar solutions. The dielectric constant decreases with the increase in salt and sugar contents in the solution. In [3], the dielectric properties change due to the bond of dissolved ions and water molecules when salt is added to the water. This change reduces the polarization of water and decreases the dielectric constant. The molecules of the sugar bond with the free molecules of water after adding sugar in water, thereby reducing the polarization of water molecules and decreasing the dielectric constant when sugar is added to water. The effective dielectric constant also decreases given the dielectric constant decrement. Therefore, the load impedance decreases, and consequently, the reflection coefficient decreases.

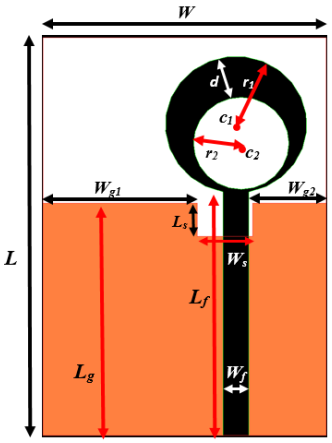

FIGURE 1. The layout of the presented antenna structure.

III. MATERIALS AND SOLUTION PREPARATION

A. ANTENNA DESIGN AND PARAMETRIC SWEEP

The design of a compact antenna, which exhibits minimal distortion in a large frequency range, remains a challenge. Figure 1 illustrates the presented crescent-shaped microstrip patch antenna. The antenna is composed of a crescent-shaped patch with the slotted partial ground plane.

The microstrip patch of the presented antenna is printed on one side of an FR4 substrate. The substrate has a compact size of L × W with a thickness of 1.6 mm and a relative permittivity of 4.6 and 0.02 loss tangent. A microstrip line with length L_f and width W_f is printed on the same side of the substrate material, which acts as a radiating component. The slotted partial ground plane is printed on the opposite side of the FR4 material. The radiating patch of the antenna is composed of a crescent-shaped patch to achieve maximum bandwidth. An SMA connector is attached to the base of the 50 Ω microstrip feed line. The change in the patch structure of the antenna causes the change in capacitance and inductance of the input impedance, for which the frequency band changes. The size and structure of the microstrip patch can control the resonance characteristics of the radiator because this structure influences the coupling between the patch and the slotted partial ground.

A parametric study is conducted to investigate the properties of the specific design of the presented antenna. The electrical and geometrical parameters affect the antenna performances. The parameters selected include the ground plane length, the presence of a slot on the ground, the presence of a hole in the radiating patch, and the outer radius of the patch. The geometric parameters of the antenna can be adjusted to achieve the return loss over a wide bandwidth. The crescent shape of the patch with the slotted partial ground can produce multiple resonances providing extensive

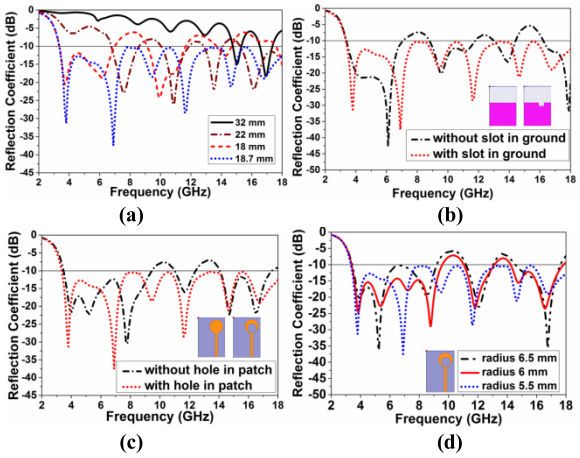

FIGURE 2. (a) Simulated S11 for a different length of the ground plane (Lg) (b) S11 for the presence of slot on the ground plane (c) S11 for the presence of the hole in the patch (d) S11 for different values of the outer radius of the patch.

bandwidth. The effects of changing the ground plane length (L_g), the presence of the slot on the ground, circular-shaped patch with a hole, and outer radius of the patch were investigated; these parameters are crucial to impedance matching. These parameters are studied in the simulations, whereas the other parameters remain constant.

The length of the ground plane has a significant role in the wideband antenna design. Figure 2(a) presents the reflection coefficient for the different ground plane lengths. The impedance bandwidth depends on the ground plane length. The ground plane length is significant at lower frequencies, where the current is concentrated for impedance matching. The variation in the ground plane lengths at certain values causes bandwidth reduction. In Figure 2(a), the ground plane length of 18.7 mm has an improved impedance bandwidth from 3.20 GHz to more than 18.0 GHz with a VSWR $\leq$2. Figure 2(b) depicts the effect of the presence of a slot on the ground plane on impedance matching. In this figure, the slot on the ground plane plays a vital role in increasing impedance bandwidth because of the electromagnetic coupling between the slotted ground plane and the radiating patch. Figure 2(c) displays the effects of the presence of a hole in the radiating patch on impedance matching. The hole in the patch has a negligible effect at lower frequencies, but the effects are more significant at higher frequencies (at least 9 GHz). The current fed by feed line is equally distributed on the patch when the patch is not carved out by the inner circle. However, the patch size and shape are changed when an inner circle is carved out from the outer circle; hence the current is unequally distributed over the patch. This unequal current distribution increases the radiation at higher frequencies to promote impedance bandwidth. The effects of the various outer radius of the patch on the reflection coefficient are illustrated in Figure 2(d). In this figure, impedance bandwidth reduces by varying the radius of the patch from a certain value. The optimized value of the outer radius for the presented wideband antenna is 5.5 mm.

FIGURE 3. Samples of the different concentrated solution. (a) salt (b) sugar.

The asymmetric structure of the patch and the offset feed line from the center of the substrate play a significant role in impedance matching. The asymmetry of the patch structure in terms of the substrate forms the coupling between the patch and the ground. Consequently, the low frequency moves into the low band, and the high frequency moves into the high band, thereby enhancing the impedance bandwidth. The feed line produces an impedance matching circuit when it is offset from the center of the substrate. This circuit has negative capacitance; hence the impedance becomes approximately 50 Ω. For these asymmetric design properties, the presented antenna covers an extensive bandwidth from 3.2 GHz to more than 18.0 GHz, as illustrated in Figure 2. The optimized parameters of the presented antenna are as follows: $L = 32$ mm, $W = 22$ mm, $L_g = 18.70$ mm, $L_f = 19.50$ mm, $W_{g1} = 12.05$ mm, $W_{g2} = 5.65$ mm, $W_f = 2.00$ mm, $L_s = 2.70$ mm, $W_s = 4.30$ mm, $r_1 = 5.5$ mm, $r_2 = 3.7$ mm, and $d = 3.40$ mm.

B. SOLUTION PREPARATION

Salt (NaCl) and sugar ($C_{12}H_{22}O_{11}$) are crystalline compounds. These compounds can easily dissolve in water and appear in an ionic state. For the experiment, salt and sugar are added individually to water to make a 20%, 40%, 60%, and 80% salt and sugar solution. Figure 3 depicts the samples of various concentrated solutions of salt and sugar.

IV. EXPERIMENTED RESULT AND DISCUSSIONS

A. ANALYSIS OF ANTENNA PERFORMANCES

The presented crescent-shaped microstrip patch antenna has been simulated with the high-frequency structure simulator and validated with the computer simulation technology (CST). The antenna has been fabricated on the printed circuit board for practical measurement. The measurement has been performed in the microwave laboratory at the Department of Electrical, Electronic & Systems Engineering (JKEES), UKM, Malaysia. N5227A PNA microwave network analyzer (10 MHz–67 GHz) and SATIMO near-field measurement system (measurement range 1.0–18.0 GHz) have been used for measuring the presented antenna. The simulated and measured results have been plotted by using OriginPro. Figure 4 displays the images of the top view, bottom view, and PNA and SATIMO measurements during the measurement of the fabricated prototype.

Figure 5 exhibits the simulated and measured reflection coefficients of the presented antenna against the

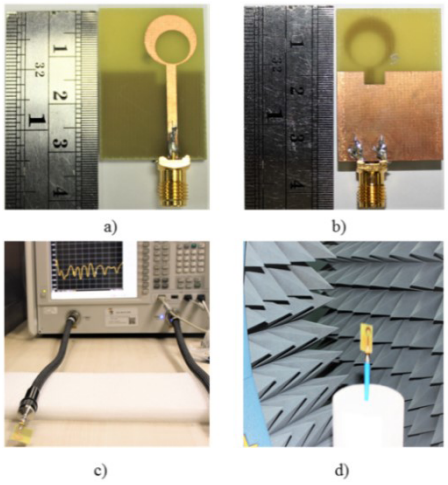

FIGURE 4. Picture of the presented prototype. (a) Top view (b) Bottom view (c) PNA measurement (d) Satimo measurement.

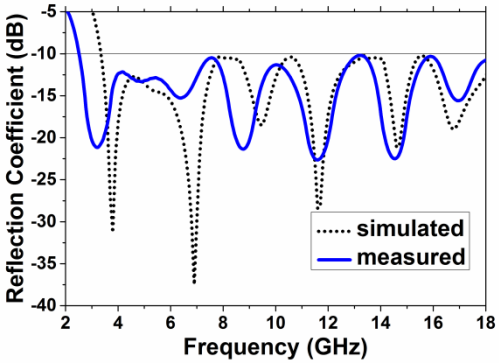

FIGURE 5. Simulated and measured reflection coefficient of the presented antenna.

frequency. According to the simulation, the presented antenna achieves impedance bandwidths from 3.20 GHz to more than 18.0 GHz to maintain a VSWR $\leq$ 2, whereas the impedance bandwidth in the measurement is from 2.50 GHz to 18.0 GHz, thus generating six resonant frequencies at 3.2, 6.3, 8.7, 11.6, 14.5, and 17.0 GHz with a reflection coefficient of −21.4, −15.45, −21.6, −23.0, −22.7, and −15.7 dB, respectively. The slot on the partial ground plane plays a vital role in increasing impedance bandwidth because of the electromagnetic coupling between the slotted partial ground plane and the radiating patch. Again, the asymmetric design of the crescent-shaped patch has a vital role to promote impedance bandwidth. The current fed by feed line is unequally distributed over the patch due to the crescent-shaped design. This unequal current distribution increases the radiation at higher frequencies to promote impedance bandwidth. Moreover, the off-setted feed line produces an impedance matching circuit. This circuit has negative capacitance for which the impedance becomes approximately 50 Ω. For these asymmetric design properties of the antenna and off-setted feed line, the impedance matching, and the entire bandwidth are improved. The results are uniform over the

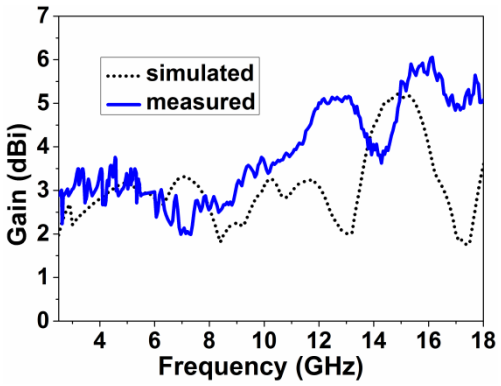

FIGURE 6. Simulated and measured gain of the presented antenna.

entire band, although minimal inconsistencies were observed between the reflection coefficients during the simulation and measurement. The inconsistency between the simulated and measured results occurs given the fabrication tolerance and feeding cable. The simulated and measured gains of the presented antenna are reflected in Fig. 6. In this figure, the antenna has 3.65 dBi average gain with a maximum gain of 6.10 dBi. The simulated and measured efficiencies of the presented antenna are illustrated in Figure 7. The antenna radiation efficiency is measured in SATIMO StarLab System. The SATIMO StarLab System measures the antenna based on a network analyzer, including near-field measurements. The near-field measurement is presented in Fig. 4d. In the SATIMO StarLab System, the electric field of the antenna is analyzed through the near-field measurement method. In this system, the data become far-field considering the strongest forces of electromagnetic induction in this field. The near-field is familiar with the Fresnel region, and it is mathematically expressed by Equation 1.

$$0.62\sqrt{\frac{D^3}{\lambda}} < R < \frac{2D^2}{\lambda}, \tag{1}$$

Where, R and D correspond to the far-field area and the maximum linear dimension of the antenna. The far-field data are found in near-field data by using a Fourier transform, which produces the radiation pattern. The near-field measurement system consists of three mechanisms, such as 16 identical measurement probes, a test board for holding the antenna in the center, and a network analyzer. The radiation pattern is measured by using the 360 ° horizontally rotating values of the antenna and an array of the 3D scan values of the probe. Then, the radiation efficiency is calculated using the far-field data of the radiation pattern. The presented antenna obtains an average radiation efficiency of 81% in the simulation. However, the antenna in the measurement provides 75% of radiation efficiency. This high radiation efficiency indicates that radiated power is higher than the retained power in the antenna, thereby leading to a cooler antenna. Consequently, the antenna can be used for the extended duration without performance degradation.

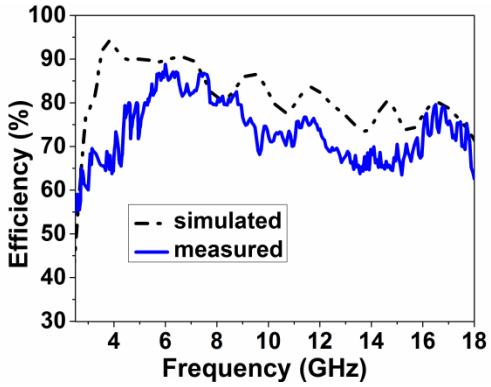

FIGURE 7. Simulated and measured efficiency of the presented antenna.

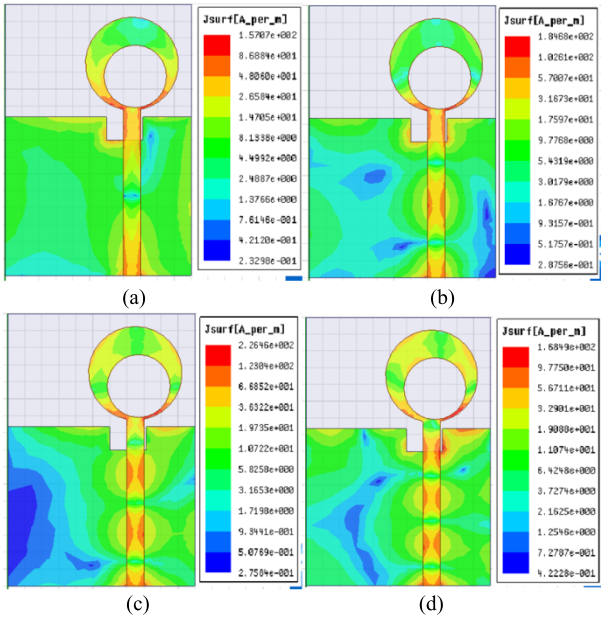

FIGURE 8. Distribution of surface current of the presented antenna at (a) 3.2 GHz (b) 8.7 GHz (c) 11.6 GHz (d) 14.5 GHz.

The current distributions on the surface of the presented antenna at four peak resonance frequencies of 3.2, 8.7, 11.6, and 14.5 GHz are depicted in Figure 8(a)–(d), correspondingly. The overlap of adjacent modes with each other is required to achieve a wideband in antenna designs. In the figures, the number of resonance increases with the operating frequency. The overlap of the resonance modes causes the current distribution of several modes. The presented antenna achieves the wideband because the surface current maintains a harmonic order of flow in the radiating crescent-shaped patch and slotted partial ground plane.

Figure 8(a) presents the current distribution at the first resonance at 3.2 GHz. The current distribution pattern at the second resonance at 8.7 GHz is depicted in Figure 8(b), thus indicating a second-order harmonic result. The complicated current distribution of 11.5 GHz corresponding to the third-order harmonic result is illustrated in Figure 8(c). The surface current has a complicated distribution pattern at 14.5 GHz corresponding to the fourth-order harmonic result, as depicted in Figure 8(d). In this figure, the current is mainly distributed along the microstrip feed line and radiating patch. The ground plane near the feed line and patch acts as the radiating plane. Moreover, the current at lower frequencies maintains a symmetrical distribution on the radiator, but the current distribution at higher frequencies is asymmetrical on the radiator.

The measured radiation pattern with co- and cross-polarization of the presented hyperband crescent-shaped, slotted partial ground microstrip patch antenna for the same frequencies in the xz-plane or E-plane ($\varphi = 0$) and yz-plane or H-plane ($\varphi = 90$) are displayed in Figure 9(a)–(d). The radiation pattern of the presented antenna at 3.2 GHz is omnidirectional in the E- and H-planes. The radiation pattern of the presented antenna at a frequency of 8.7 GHz remains sufficiently durable to be omnidirectional. The radiation pattern of the presented antenna turns directive at high frequencies of 11.6 and 14.5 GHz for the high-order current excitation. The omnidirectional pattern becomes directive at high frequencies due to several factors. First, the order of slot resonance increases with the increase in the frequency. Second, the patch at high frequencies resonates by itself.

Third, the microstrip feed line resonates at high frequencies. The results in Figure 9(a)–(d) illustrate that the radiation patterns are robust over the entire operating bandwidth.

Figure 10 displays the group delay of the presented, crescent-shaped slotted partial ground microstrip patch antenna. The minimal distorted group delay is a valuable time domain characteristic of the wideband antenna. Group delay is measured as the transit time of a pulse signal through a device versus the frequency. Pulse signals are delayed while transiting through a device or a medium. Group delay is expressed as the negative derivative of the phase to the frequency. Mathematically, group delay is represented as

$$GD = -\frac{d\varphi}{d\omega}, \tag{2}$$

Where, φ and ω denote the phases in radians and angular frequencies, respectively. Two antennas are connected to the two ports of the PNA to measure the group delay of the presented crescent-shaped antenna. In this work, it is investigated through experiments in face-to-face and side-by-side orientations. In both cases, the two antennas are positioned at 250 mm away from each other. The phase of the transmitted signal S_{21} from one antenna to another antenna is measured by the PNA. Then, the group delay is determined as the derivative of the phase versus the frequency. In this figure, a minimal inconsistency between the face-to-face and side-by-side group delays from 3.6 GHz to 5.3 GHz given the comparatively high reflection depicted in the reflection coefficient in Figure 5. The group delays during side-by-side and face-to-face positions, except for the abovementioned discrepancy, are nearly the same and linear. The group

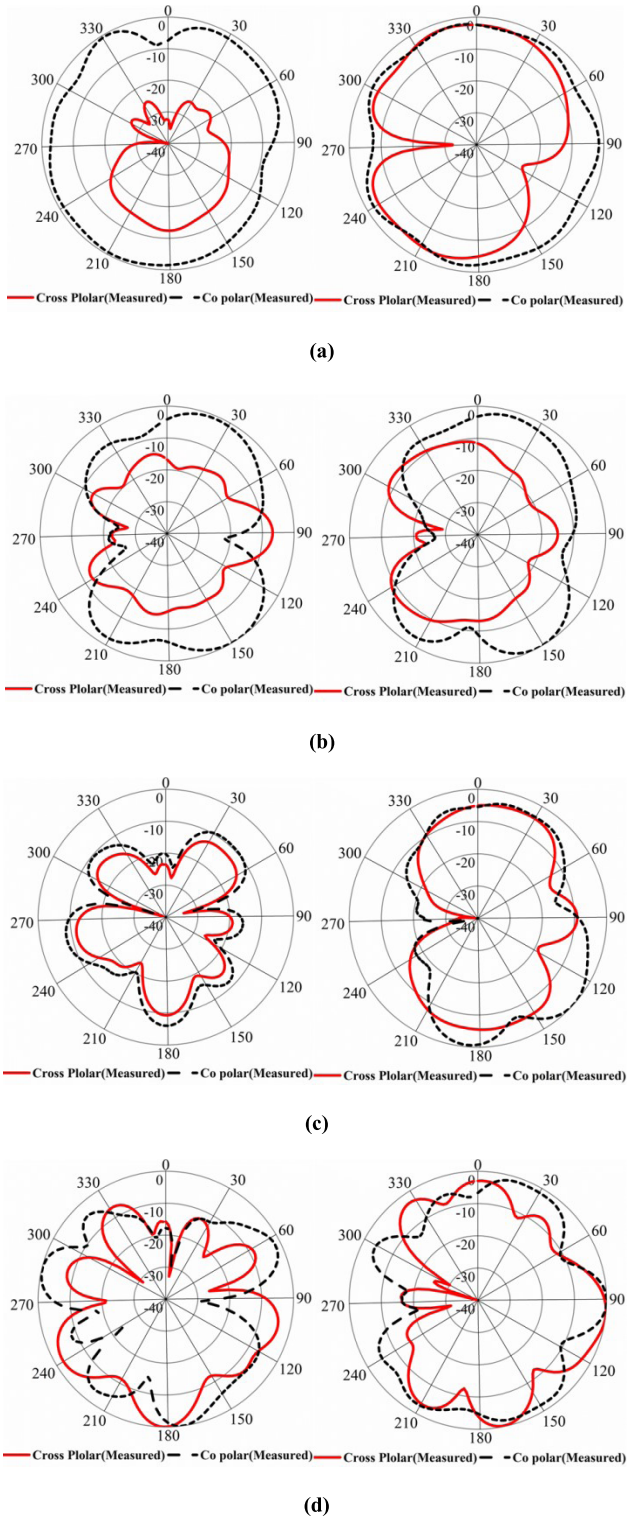

FIGURE 9. Radiation Pattern of the presented antenna at (a) 3.2 GHz (b) 8.7 GHz (c) 11.6 GHz (d) 14.5 GHz.

delay corresponds well to the transmission characteristics of the presented antenna, thereby proving a minimal signal distortion.

Figure 11 presents the measured phase of the input impedance of the presented antenna. In this figure, the phase

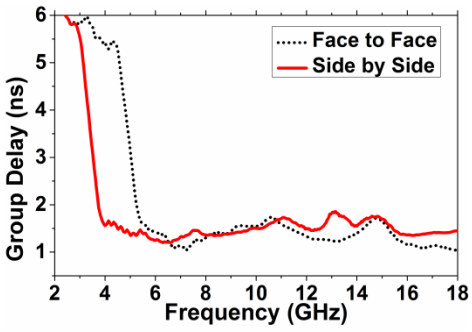

FIGURE 10. Group Delay of the presented antenna.

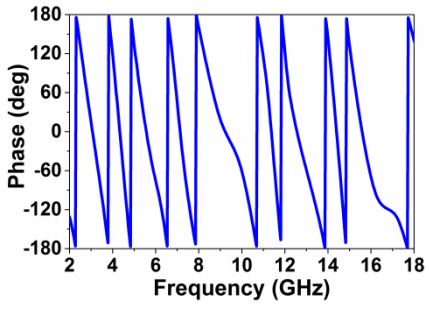

FIGURE 11. Phase of the input impedance.

variation of the antenna is linear throughout the operating band. The linear phase variation with frequencies affirms the same delay, thus leading to the same pulse distortions in all frequency components of the signal.

The output pulse at the receiving antenna is the convolution of the transfer function and input pulse. The transfer function is transformed into the time domain by using inverse Fourier transform. Figure 12 depicts the input and output pulses when the antennas are in the face-to-face and side-by-side orientations. In both cases, the distance between the antennas is 250 mm. In this figure, the input and received pulses are similar in the side-by-side orientation. Therefore, the antenna can radiate a short pulse with negligible distortion. The received pulse in the face-to-face orientation is slightly distorted from the input pulse given the fine energy storage effects of the lossy FR4 substrate. The fidelity parameter is used to estimate the signal distortion. Fidelity is the peak magnitude of the cross-correlation between input and received pulses. Equation 3 is used to find the fidelity factor, which has been described in [1].

$$F = \max \frac{\int_{-\infty}^{+\infty} x(t)\, y(t+\tau)\, dt}{\sqrt{\int_{-\infty}^{+\infty} |x(t)^2|\, dt \int_{-\infty}^{+\infty} |y(t)^2|\, dt}}, \tag{3}$$

Where, x (t) and y (t) are the input and received pulses, correspondingly. The fidelity factor for the face-to-face and side-by-side orientations of the presented antenna is determined to be 0.7916 and 0.8004, respectively, by using Equation 3. The distortion of the pulse in the antenna is low when the fidelity factor value is high.

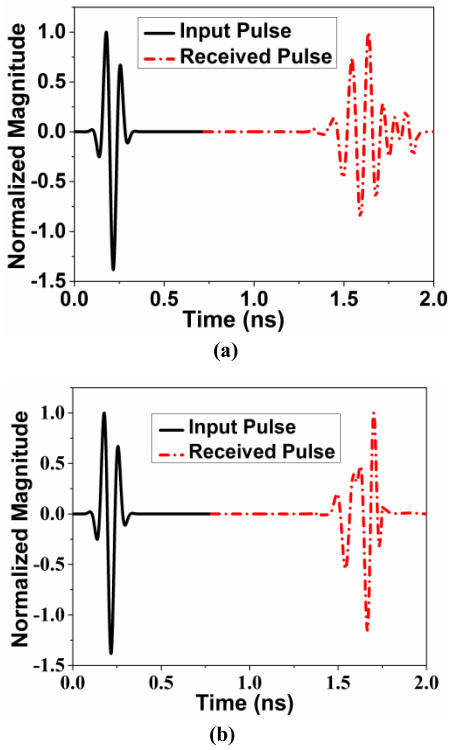

FIGURE 12. Input and received pulses (a) Face to Face orientation (b) Side by side orientation.

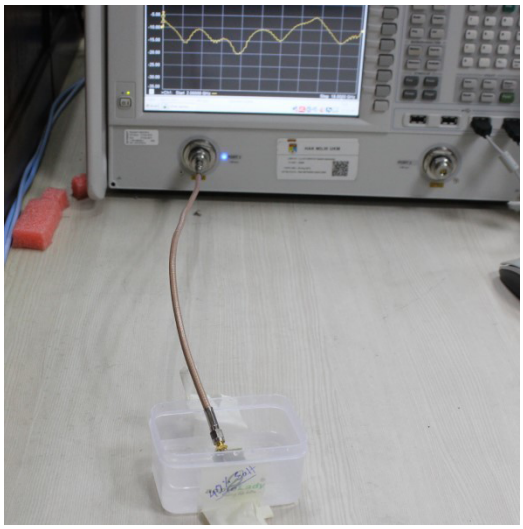

FIGURE 13. Measurement setup of the proposed antenna as a sensor.

B. SENSOR APPLICATION AND DISCUSSION

For the practical investigation of the presented antenna as a sensor, the reflection coefficient of the antenna has been measured using the N5227A PNA Microwave Network Analyzer (10MHz–67GHz) at the microwave laboratory in JKEES. The reflection coefficient of the antenna has been measured in free space and with the different salt and sugar concentrations to detect the salt and sugar contents in water. The measurement setup is displayed in Figure 13.

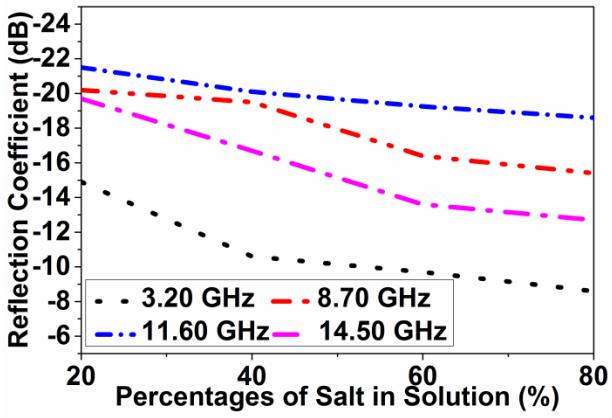

FIGURE 14. Reflection coefficient variation with the different percentage of salt in water.

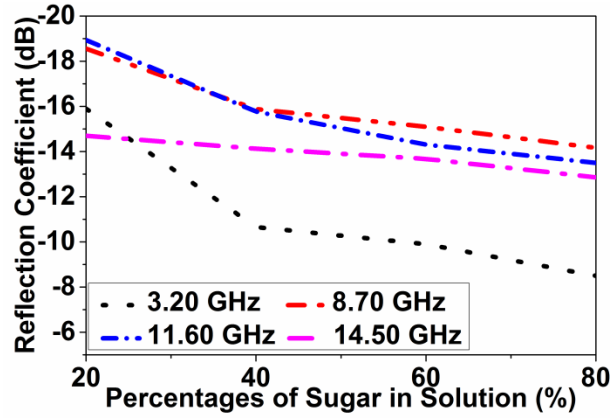

FIGURE 15. Reflection coefficient variation with the different percentage of sugar in water.

The sensor has been investigated using various concentrated solutions of salt and sugar. The solutions have been divided into two categories. The first category contains four samples of salt, concentrated at 20%, 40%, 60%, and 80%. The second category contains four samples of the same concentrations of sugar solutions. The two categories are presented in Figure 3. The reflection coefficient variation at the peak resonance frequencies at 3.2, 8.7, 11.6, and 14.5 GHz with the percentage of salt and sugar concentrations in water are illustrated in Figure 14 and Figure 15, respectively.

In these figures, the reflection coefficients decrease with the increase in the percentages of salt and sugar in water. The free water molecules decrease with the increment of salt and sugar content in water. The dielectric properties change due to the bond of the dissolved ions and water molecules when the salt and sugar content is added to the water. This change reduces the polarization of water due to the decrement of ionic conductivity of the solution. When the concentration of salt and sugar increases in water, the free water molecules decrease and hence the ionic conductivity of the solution also decreases. This decrement of ionic conductivity causes the decrement of the dielectric constant of the solution which leads to the reduction of the effective dielectric constant

TABLE 1. Reflection coefficients for the different concentrated salt in water at different frequencies.

Frequency (GHz)	Concentration			
	20%	40%	60%	80%
3.20	-14.90 dB	-10.60 dB	-9.70 dB	-8.60 dB
8.70	-20.20 dB	-19.50 dB	-16.4 dB	-15.40 dB
11.60	-21.50 dB	-20.10 dB	-19.25 dB	-18.60 dB
14.50	-19.70 dB	-16.70 dB	-13.60 dB	-12.70 dB

TABLE 2. Reflection coefficients for the different concentrated sugar in water at different frequencies.

Frequency (GHz)	Concentration			
	20%	40%	60%	80%
3.20	-15.90 dB	-10.66 dB	-9.90 dB	-8.50 dB
8.70	-18.56 dB	-15.88 dB	-15.10 dB	-14.17 dB
11.60	-18.94 dB	-15.77 dB	-14.31 dB	-13.50 dB
14.50	-14.70 dB	-14.13 dB	-13.68 dB	-12.86 dB

of the solution. The load impedance also decreases given a decrement in the effective dielectric constant of the solution. Thus, due to the decrement of load impedance, the reflection coefficient decreases.

The reflection coefficients for the various salt concentrations in water are summarized in TABLE 1. The reflection coefficients for the different sugar concentrations in water are listed in TABLE 2. TABLE 1 and TABLE 2 display that the reflection coefficients decrease with the increase in the percentages of salt and sugar concentrations in water.

V. CONCLUSION

A low-profile crescent-shaped microstrip antenna-based sensor for detecting salt and sugar concentrations in water is presented in this paper. The antenna has a compact size of 32 mm $\times$ 22 mm on a low-cost FR4 PCB substrate. The antenna achieves a maximum gain of 6.10 dBi with high efficiency. The fidelity factor for the face-to-face and side-by-side orientations of the presented antenna is found to be 0.7916 and 0.8004, respectively. The radiation patterns of the antenna are robust throughout the operating band; hence the antenna is suitable for wireless communication and sensor applications. The measurements of reflection coefficient within the salt and sugar solution demonstrate that the reflection coefficients decrease with the increment in percentages of salt and sugar concentrations in water. This phenomenon occurs because of the decrement in the dielectric constant and loss of water molecules. The experiments show that the presented sensor exhibits a favorable sensitivity for detecting salt and sugar contents in water. This low-cost measurement system can be used in the food and beverage industry to detect the salt and sugar concentrations in food or beverage because the quantity of salt and sugar concentrations in food and beverage is compulsory under the law.

REFERENCES

[1] K. L. Gartley, "Recommended methods for measuring soluble salts in soils," *Recommended Soil Test. Procedures Northeastern United States. Cooperat. Bull*, vol. 493, pp. 87–94, 2011.

[2] C. Bircan and S. A. Barringer, "Salt-starch interactions as evidenced by viscosity and dielectric property measurements," *J. Food Sci.*, vol. 63, no. 6, pp. 983–986, 1998.

[3] D. H. Gadani, V. A. Rana, S. P. Bhatnagar, A. N. Prajapati, and A. D. Vyas, "Effect of salinity on the dielectric properties of water," *Indian J. Pure Appl. Phys.*, vol. 50, pp. 405–410, Jun. 2012.

[4] C. Deffendol and C. Furse, "Microstrip antennas for dielectric property measurement," in *Proc. IEEE Antennas Propag. Soc. Int. Symp.*, Jul. 1999, pp. 1954–1956.

[5] R. Zajıcek, T. Smejkal, L. Oppl, and J. Vrba, "Medical diagnostics using reflection method and waveguide probes-feasibility study," in *Proc. Prog. Electromagn. Res. Symp.*, Cambridge, MA, USA, Jul. 2008, pp. 759–762.

[6] Z. Abbas, R. Mokhtar, K. Khalid, M. Hashim, and S. A. Aziz, "RDWG technique of determination of moisture content in oil palm fruits," *Eur. Phys. J. Appl. Phys.*, vol. 40, pp. 207–210, Nov. 2007.

[7] K. Khalid, "The application of microstrip sensors for determination of moisture content in Hevea Rubber Latex," *J. Microw. Power Electromagn. Energy*, vol. 23, pp. 45–51, Jun. 1988.

[8] M. M. Ghretli, K. Khalid, I. V. Grozescu, M. H. Sahri, and Z. Abbas, "Dual-frequency microwave moisture sensor based on circular microstrip antenna," *IEEE Sensors J.*, vol. 7, no. 12, pp. 1749–1756, Dec. 2007.

[9] N. Yahaya, Z. Abbas, M. Ismail, and B. M. Ali, "Determination of moisture content of hevea rubber latex using a microstrip patch antenna," in *Proc. Prog. Electromagn. Res. Symp. (PIERS)*, 2012, pp. 1290–1293.

[10] T. J. Harpster, B. Stark, and K. Najafi, "A passive wireless integrated humidity sensor," *Sens. Actuators A, Phys.*, vol. 95, pp. 100–107, Jan. 2002.

[11] W. Withayachumnankul, K. Jaruwongrungsee, A. Tuantranont, C. Fumeaux, and D. Abbott, "Metamaterial-based microfluidic sensor for dielectric characterization," *Sens. Actuators A, Phys.*, vol. 189, pp. 233–237, Jan. 2013.

[12] I. M. Rusni, A. Ismail, A. R. H. Alhawari, M. N. Hamidon, and N. A. Yusof, "An aligned-gap and centered-gap rectangular multiple split ring resonator for dielectric sensing applications," *Sensors*, vol. 14, no. 7, pp. 13134–13148, Jan. 2014.

MOHAMMAD TARIQUL ISLAM (M'08–SM'13) is currently a Professor with the Department of Electrical, Electronic and Systems Engineering, Universiti Kebangsaan Malaysia (UKM) and a Visiting Professor with the Kyushu Institute of Technology, Japan. He has authored over 350 research journal articles, over 165 conference articles, four research level books, and a few book chapters on various topics related to antennas, microwaves and electromagnetic radiation analysis with 13 inventory patents filed. Thus far, his publications have been cited 3416 times and his H-index is 30 (Source: Scopus). His Google scholar citation is 9993 and H-index is 35. He is currently involved in many research projects through the Malaysian Ministry of Science, Technology and Innovation and Ministry of Education. His research interests include communication antenna design, radio astronomy antennas, satellite antennas, and electromagnetic radiation analysis. He received several International Gold Medal Awards, the Best Invention in Telecommunication Award, a Special Award from Vietnam for his research and innovation, and the Best Researcher Awards in 2010 and 2011 at UKM. He also received the Best Innovation Award in 2011 and the Best Research Group in ICT niche in 2014 by UKM. He was the recipient of Publication Award from Malaysian Space Agency in 2014, 2013, 2010, 2009 and the Best Paper Presentation Award in 2012 International Symposium on Antennas and Propagation, Nagoya, Japan and in 2015 in Icon Space. He is a Chartered Professional Engineer-CEng, Member of IET (U.K.) and member of IEICE, Japan. He currently serves as the Editor-in-Chief for the *International Journal of Electronics and Informatics* and an Associate Editor for the *International Journal of Antenna and Propagation and Electronics Letter*.

MD. NAIMUR RAHMAN received the B.Sc. (Engg.) degree in computer science and engineering from Patuakhali Science and Technology University (PSTU), Bangladesh. He is pursuing the master's degree with the Universiti Kebangsaan Malaysia (UKM), Malaysia. He is also an Assistant Professor with the Electrical and Electronics Engineering Department, PSTU. He has authored or co-authored a number referred journals and conference papers. He is currently a Graduate Research Assistant with the Department of Electrical, Electronic and Systems Engineering, UKM, Malaysia. His research interests include the antenna design, satellite communication, and wireless communication.

MANDEEP SINGH JIT SINGH received the B.Eng. degree (Hons.) and the Ph.D. degree in electrical and electronic engineering from the University of Notrhumbria, U.K., and Universiti Sains Malaysia, in 1998 and 2006, respectively. From 2006 to 2009, he was at Universiti Sains Malaysia as a Lecturer. He is currently an Associate Professor with the Universiti Kebangsaan Malaysia. His areas of specialization are radiowave propagation in satellite communication system, and RFID antenna design. He is collaborated with the Association of Radio Industries and Business, Japan to analyze the rain fade at Ku-band in tropical climate using satellite involving countries, such as Thailand, Philippines, Indonesia, and Fiji. His current collaboration is with National Defense Agency, Japan, Microwave Anechoic Lab Chamber, and Kyutech University on antenna development. He has published 190 papers in ISI journals. He has reviewed over 200 articles in impact factors journal.

MD. SAMSUZZAMAN was born in Jhenaidah, Bangladesh, in 1982. He received the B.Sc. and M.Sc. degrees in computer science and engineering from Islamic University Kushtia, Bangladesh, in 2005 and 2007, respectively, and the Ph.D. degree from the Universiti Kebangsaan Malaysia, Malaysia, in 2015. From 2008 to 2011, he was a Lecturer at Patuakhali Science and Technology University (PSTU), Bangladesh. From 2011 to 2015, he was an Assistant Professor at the PSTU. He is currently as an Associate Professor with PSTU. He has authored or co-authored approximately 68 referred journals and conference papers. His research interests include the communication antenna design, microwave imaging, satellite antennas, and satellite communication.